JACS
JOURNAL OF THE AMERICAN CHEMICAL SOCIETY
Article
pubs.acs.org/JACS

Identifying the Molecular Structures of Intermediates for Optimizing the Fabrication of High-Quality Perovskite Films

Jing Cao,[†,§] Xiaojing Jing,[†,§] Juanzhu Yan,[†] Chengyi Hu,[†] Ruihao Chen,[†] Jun Yin,[†,‡] Jing Li,*[,‡] and Nanfeng Zheng*[,†]

[†]State Key Laboratory for Physical Chemistry of Solid Surfaces, Collaborative Innovation Center of Chemistry for Energy Materials, Engineering Research Center for Nano-Preparation Technology of Fujian Province, College of Chemistry, Chemical Engineering, Xiamen University, Xiamen 361005, China

[‡]Collaborative Innovation Center for Optoelectronic Semiconductors, Efficient Devices, Pen-Tung Sah Institute of Micro-Nano Science, Technology, Xiamen University, Xiamen 361005, China

Supporting Information

ABSTRACT: During the past two years, the introduction of DMSO has revolutionized the fabrication of high-quality pervoskite $MAPbI_3$ (MA = CH_3NH_3) films for solar cell applications. In the developed DMSO process, the formation of $(MA)_2Pb_3I_8{\cdot}2DMSO$ (shorted as Pb_3I_8) has well recognized as a critical factor to prepare high-quality pervoskite films and thus accomplish excellent performances in perovskite solar cells. However, Pb_3I_8 is an I-deficient intermediate and must further react with methylammonium iodide (MAI) to be fully converted into $MAPbI_3$. By capturing and solving the molecular structures of several intermediates involved in the fabrication of perovskite films, we report in this work that the importance of DMSO is **NOT** due to the formation of Pb_3I_8. The use of different PbI_2-DMSO ratios leads to two different structures of PbI_2-DMSO precursors ($PbI_2{\cdot}$DMSO and $PbI_2{\cdot}$2DMSO), thus dramatically influencing the quality of fabricated perovskite films. However, such an influence can be minimized when the PbI_2-DMSO precursor films are thermally treated to create mesoporous PbI_2 films before reacting with MAI. Such a development makes the fabrication of high-quality pervoskite films highly reproducible without the need to precisely control the PbI_2:DMSO ratio. Moreover, the formation of ionic compound $(MA)_4PbI_6$ is observed when excess MAI is used in the preparation of perovskite film. This I-rich phase heavily induces the hysteresis in PSCs, but is readily removed by isopropanol treatment. On the basis of all these findings, we develop a new effective protocol to fabricate high-performance PSCs. In the new protocol, high-quality perovskite films are prepared by simply treating the mesoporous PbI_2 films (made from PbI_2-DMSO precursors) with an isopropanol solution of MAI, followed by isopropanol washing. The best efficiency of fabricated $MAPbI_3$ PSCs is up to 19.0%. As compared to the previously reported DMSO method, the devices fabricated by the method reported in this work display narrow efficiency distributions in both forward and reverse scans. And the efficiency difference between forward and reverse scans is much smaller.

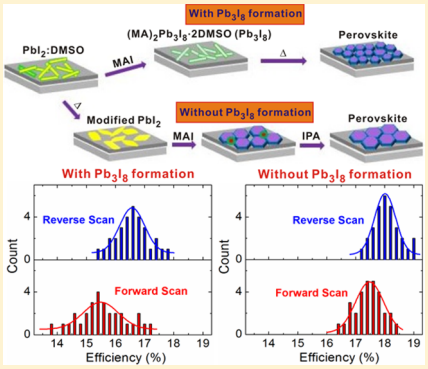

INTRODUCTION

Perovskite solar cells (PSCs) have been emerging as one of the most promising candidates for next generation solar cells in view of their high efficiency, simple solution-processed technique and low cost.[1−10] Enormous researches have been devoted to develop various approaches for continuous improvement of PSCs' performance. For example, interface engineering has been extensively attempted to optimize the contacts of perovskite layer with the electron or hole transport layers.[11−16] Together with the composition of perovskites,[10,17−19] the quality control over the perovskite films has also attracted much research attention.[10,20−27] Recently, a certified PSCs' efficiency over 20% was achieved by introducing dimethyl sulfoxide (DMSO) into perovskite precursor solution to prepare high quality perovskite films.[10] Studies revealed that, as a coordinative solvent for PbI_2, the involvement of DMSO retarded the reaction of PbI_2 and methylammonium iodide (MAI), and thus helped to improve the quality of fabricated perovskite films.[28−31] However, it has been noted that the amount of DMSO introduced in the system was very critical. The molar ratio of PbI_2:DMSO was found to be constrained to a quite narrow window around 1:1.[30,31] It still remains unclear why the PbI_2:DMSO ratio could not be extended into a much wider region to make the fabrication of high-efficient PSCs more easily controlled and reproducible.

Moreover, with the use of DMSO, an intermediate phase $(MA)_2Pb_3I_8{\cdot}2DMSO$ (denoted as Pb_3I_8) has been often identified.[32,33] Chemically, compared to perovskite, Pb_3I_8 is an I-deficient structure and needs to further react with MAI to form perovskite. Very recently, three different transition pathways from Pb_3I_8 to perovskite under different annealing

Received: May 12, 2016
Published: July 18, 2016

DOI: 10.1021/jacs.6b04924
J. Am. Chem. Soc. 2016, 138, 9919−9926

conditions have been investigated.[34] However, research effort understanding the role of Pb_3I_8 is very limited. It is still unclear whether the formation of the Pb_3I_8 intermediate is a prerequirement for the fabrication of high-quality perovskite films. The molecular understanding on how DMSO and Pb_3I_8 are involved in the formation of high-quality perovskite films is thus crucial to further improve the performance of PSCs made by the developed DMSO method.

By capturing several intermediates involved in the fabrication of perovskite films with the introduction of DMSO and resolving their molecular structures, we report in this work the molecular insight on how the amount of DMSO influences the quality of perovskite films as well as their cell performances. Systematic studies revealed that different amount of DMSO would change the form of PbI_2 and thus influence the film quality of PbI_2 precursors and their reactivity. With the PbI_2:DMSO molar ratio at 1:1, a PbI_2·DMSO complex was produced. The complex readily grew on substrates as a continuous high-quality film with small crystallite domains and thus good reactivity toward the formation of perovskite films. The formation of the Pb_3I_8 intermediate during the perovskite fabrication process is **NOT** a key factor for constructing high-efficiency PSC devices. Also, the I-rich ionic compound $(MA)_4PbI_6$ was found to form with the presence of excess MAI during preparation of perovskite film, which was evidently revealed to induce the hysteresis in corresponding PSCs. Based on these findings, a highly reproducible protocol using mesoporous PbI_2 films derived from PbI_2-DMSO complexes was developed for the preparation of high-quality perovskite film without the need to precisely control the PbI_2:DMSO molar ratio in the fabrication. Furthermore, simply treating the mesoporous PbI_2 films with an isopropanol (IPA) solution of MAI followed by IPA washing to avoid the involvement of excess ionic compound during the fabrication of perovskite films, afforded high quality perovskite films as well reproducible PSCs devices with negligible hysteresis.

RESULTS AND DISCUSSION

Figure 1a shows the typical protocol for preparing high-quality perovskite films either by one- or two-step method that involves the use of DMSO with the PbI_2:DMSO ratio of 1:1. We employed both one- and two-step methods to fabricate PSCs devices. The fabricated PSCs had a typical p-i-n configuration of FTO/TiO_2/$MAPbI_3$/Spiro-OMeTAD/Au. As shown in Figure S1, S2 and Table S1, the best cell efficiencies reached to 18.4% for one-step and 18.0% for two-step methods. A small hysteresis was still observed on the fabricated devices. However, as presented in the histograms for all independently prepared 30 cells (Figure 1b,c), rather broad distributions of overall efficiencies were revealed in the reverse scan (RS: 17.2 ± 1.2% for one-step and 16.6 ± 1.2% for two-step) and also in the forward scan (FS: 15.6 ± 2.3% for one-step and 15.5 ± 2.1% for two-step). The efficiency distribution for the forward scan was broader than that for the reverse scan.

Pb_3I_8 Intermediate. As shown in Figure S3, in both one- and two-step methods, the Pb_3I_8 phase was formed as an important intermediate before the formation of the targeted perovskite compound, consistent with previous reports.[28] Yellow single crystals of pure Pb_3I_8 phase were prepared by diffusing diethyl ether into a mixture of PbI_2 and MAI (1:1 molar ratio) in DMSO. Structurally, Pb_3I_8 can be described as triple-chains of edge-sharing PbI_6 octahedra with all unshared apexes sitting at their sides (Figure 1d). They can be considered

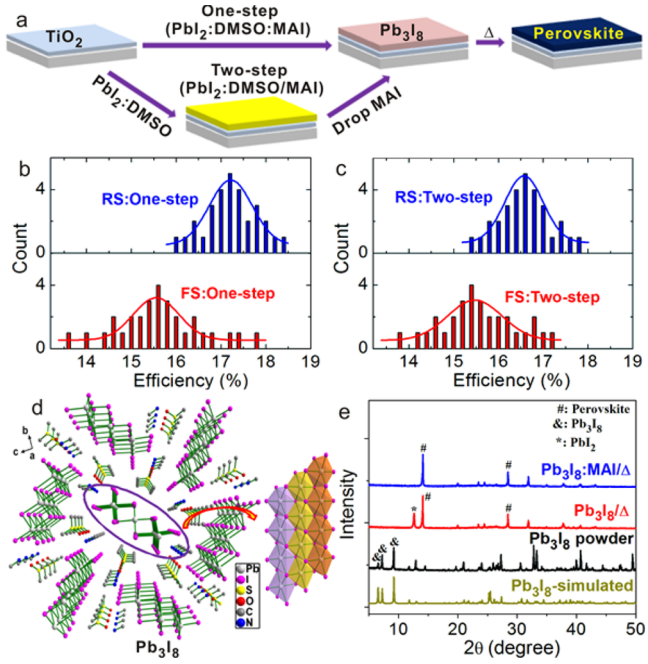

Figure 1. (a) Schematic illustration of cell fabrication process by one- and two-step methods. Histogram of efficiencies among 30 cells obtained by one- (b) and two-step (c) methods. (d) Crystal structure of Pb_3I_8. (e) XRD patterns of Pb_3I_8 powder before and after annealing, and heated sample (100 °C for 5 min) of Pb_3I_8 mixing with equimolar MAI (Pb_3I_8:MAI/Δ).

as I-terminated fragments of PbI_2. These negatively charged $\{(Pb_3I_8)_n\}^{2n-}$ chains are charge-balanced by MA cations (Figure 1d). As compared to the Pb−I molar ratio of 1:3 in perovskite, the intermediate Pb_3I_8 phase is a compositionally I-deficient phase. As expected, simple thermal annealing of pure Pb_3I_8 led to the formation of PbI_2 together with perovskite (Figure 1e). Therefore, the PSCs fabricated from pure Pb_3I_8 films exhibited poor performances (Figure S4 and Table S1). To chemically achieve the complete conversion of Pb_3I_8 into perovskite, the equimolar MAI should be introduced to react with the Pb_3I_8 phase (Figure 1e). It should be noted that in the as-prepared perovskite films made by either one- or two-step method, no PbI_2 diffraction peaks were observed after annealing (Figure S5), indicating the existence of amorphous MAI as the reactant in perovskite precursor film. The Pb_3I_8:MAI ratio is thus important to transfer Pb_3I_8 into high-quality perovskite films. However, the precise control over the local Pb_3I_8:MAI ratio is technically hard to be achieved by either one- or two-step method, which might explain why there were broad efficiency distributions in the fabricated PSCs.

Structures of PbI_2 Precursors. Considering that the secondary reaction between Pb_3I_8 and MAI is required to obtain high-quality perovskite films, we argue that the formation of Pb_3I_8 might not be necessary to reproduce high-quality perovskite films in the reported DMSO-assisted method. Improving the quality of the precursor films with the help of DMSO could be the main reason for producing high-quality perovskite films, as reflected in the perovskite films using different PbI_2:DMSO ratios by one-step method (Figure S6). Since the Pb_3I_8 phase was formed in all DMSO-precursor films before the perovskite formation in the one-step process (Figure S7), modifying the PbI_2 precursor film in two-step method may give some useful suggestions. Considering the

DOI: 10.1021/jacs.6b04924
J. Am. Chem. Soc. 2016, 138, 9919−9926

PbI_2:DMSO molar ratio was critical to fabricate efficient PSCs, we investigated in this work the detailed structures of PbI_2 intermediates using DMSO in different molar ratios by adopting two-step method. When the PbI_2:DMSO molar ratio was 1:1, the casted PbI_2 precursor films made of uniform crystalline nanorods were smooth and continuous without pinholes and cracks,[31] possessing the consistent XRD pattern with the one simulated from the crystal structure of PbI_2·DMSO (Figure 2a). Single crystals of PbI_2·DMSO were produced by

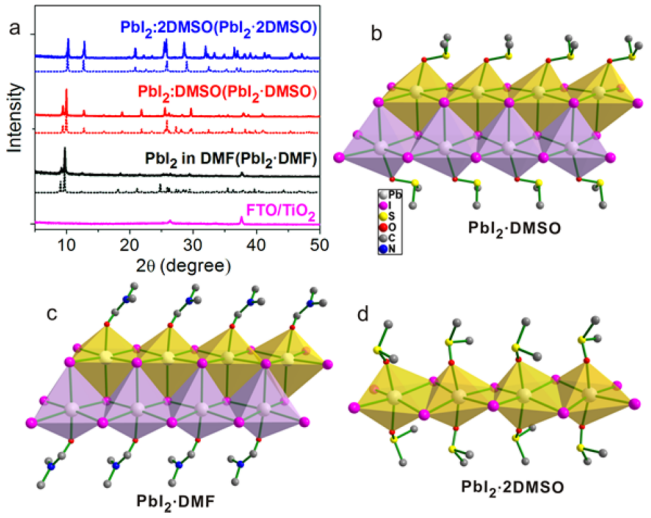

Figure 2. (a) Comparison of simulated (dot line) and experimental (solid line) XRD patterns of PbI_2 precursor films. The crystal structures of (b) PbI_2·DMSO, (c) PbI_2·DMF, and (d) PbI_2·2DMSO.

diffusing toluene into DMF solution of synthesized PbI_2·DMSO powder.[10] As revealed by X-ray single crystal analysis, the PbI_2·DMSO precursor consists of double-chains of edge-sharing PbI_5O octahedra with all unshared apexes stabilized by DMSO (Figure 2b). Such a double-chain structure can also be structurally described as DMSO-stabilized PbI_2 fragments. It should be noted that the same PbI_2 precursor structure has been previously observed by other group.[32]

A similar double-chain structure was also obtained when PbI_2 was dissolved in DMF (Figure 2c).[35] In the preparation of single crystals of PbI_2:2DMSO precursor, when toluene was slowly diffused into DMSO solution of PbI_2, another single crystal of PbI_2 precursor (PbI_2·2DMSO) with a single-chain structure made of edge-sharing PbI_4O_2 octahedra was obtained (Figure 2d).[31,36] In the structure of this single-chain precursor, DMSO molecules situate and stabilize the unshared axial trans-positions of the octahedra. A perfect match was observed between the measured XRD pattern of precursor film prepared with PbI_2:DMSO molar ratio of 1:2 and the simulated pattern from crystal structure of PbI_2·2DMSO (Figure 2a). These results suggest that the different PbI_2:DMSO ratios used in the two-step preparation of perovskite films led to the formation of PbI_2-DMSO precursors having different structures.

Essential Role of DMSO on the Film Quality of PbI_2 Precursors. Due to the much weaker binding of DMF on Pb than that of DMSO, the coordinative DMF is more easily removed from the double-chain precursor than DMSO from either one- or two-chain PbI_2 precursors as evidenced by the TGA analyses (Figure S8). The relatively strong binding of DMSO on Pb would alter the film quality of the PbI_2 precursors. As seen in Figure 3a-I, without introducing

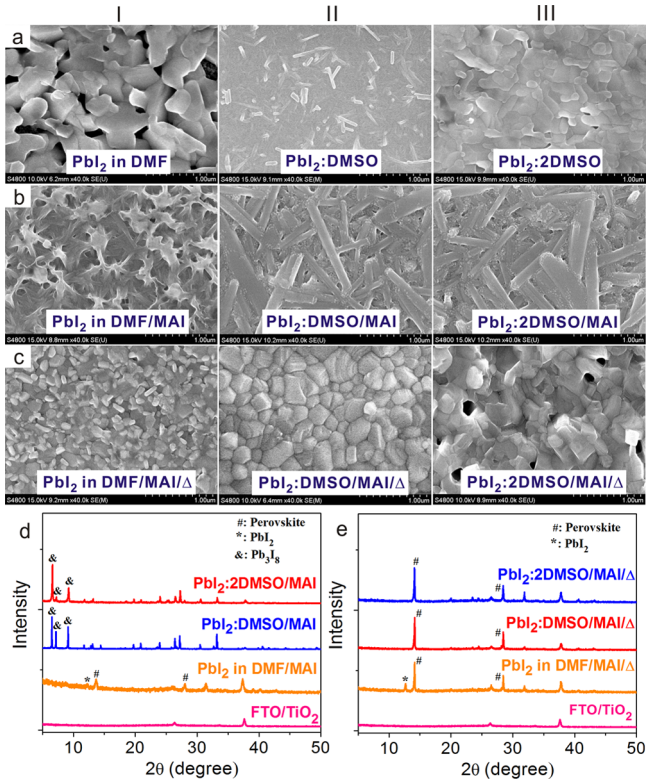

Figure 3. SEM images of PbI_2 precursor films (a) and the reaction with MAI before (b) and after (c) annealing (Δ). XRD patterns of the films obtained by reactions of PbI_2 precursors with MAI before (d) and after (e) annealing.

DMSO, the PbI_2 precursor film made in the two-step method was actually composed of large PbI_2 crystallites of ~500 nm. Then the small perovskite crystalline domains were formed on the large PbI_2 crystallites due to the easy reaction between PbI_2 and MAI (Figure 3c-I). The coverage of perovskite would then retard the further reaction of PbI_2 inside the large crystallite with MAI, often leading to the presence of untreated PbI_2 in the obtained perovskite films either without or with annealing treatments (Figure 3d,e).

In contrast, although different structures of PbI_2·DMSO and PbI_2·2DMSO formed when changing the PbI_2:DMSO ratio, the casted films were both made of much smaller crystallites, making the precursor films free of pinholes as displayed in Figure 3a-II and III. Moreover, due to the relatively strong coordination of DMSO to Pb, the reaction of both PbI_2·DMSO and PbI_2·2DMSO films with MAI led to the formation of regular rod-like Pb_3I_8 intermediate films (Figure 3b-II and III, and Figure 3d). Consequently, pure perovskite films with much larger crystalline domains than that prepared in the absence of DMSO (Figure 3c-II and III, and Figure 3e) were produced. Noticeably, in the case of perovskite films obtained by PbI_2·2DMSO precursor, although the perovskite crystallites were rather large, pinholes were still observed (Figure 3c-III). The resulting large number of pinholes might be due to the presence of large content of DMSO in the precursor films. The above observations indicate that the amount of DMSO determined the quality of perovskite films in the following two aspects: (1) It altered the film quality of PbI_2 precursors. (2) It modified the reactivity of PbI_2 precursors and thus determined the crystalline domain size in the perovskite films.

DOI: 10.1021/jacs.6b04924
J. Am. Chem. Soc. 2016, 138, 9919−9926

High-Quality Perovskite Films from Mesoporous PbI_2. To exclude the different reactivity of PbI_2 precursors, we therefore thermally treated the precursor films to convert them into mesoporous PbI_2 films with the hope that the mesoporous channels would facilitate the penetration of MAI to react with PbI_2 for forming high-quality perovskite films.[37−39] The PbI_2:DMSO and PbI_2:2DMSO precursor films were transformed into the mesoporous PbI_2 films when heated at 80 °C (Figure 4a−c and S9−S11). While a relatively dense PbI_2 film

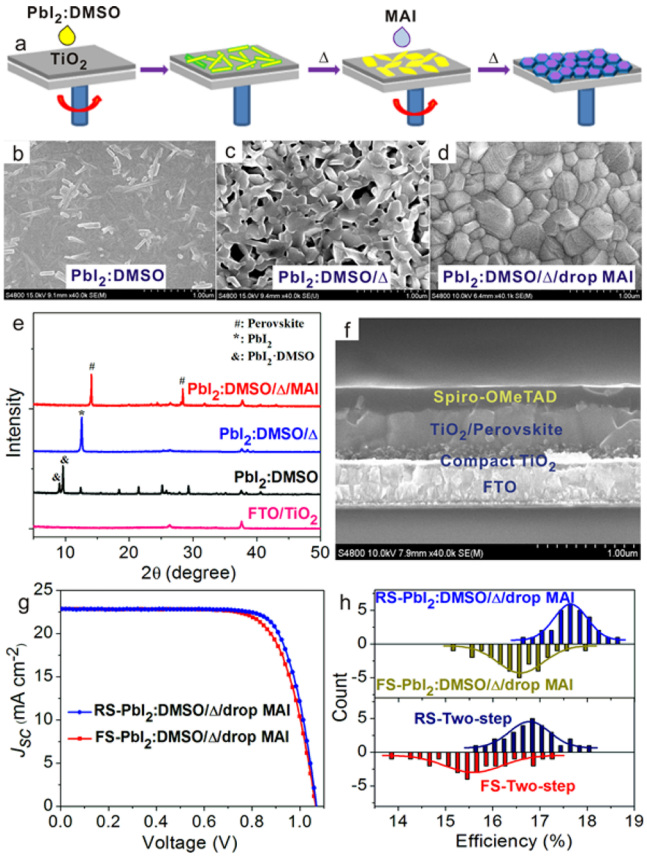

Figure 4. (a) Schematic illustration of cell fabrication process with mesoporous PbI_2 film. SEM images (b−d) and XRD patterns (e) of PbI_2·DMSO films before and after heating (Δ), and subsequently obtained perovskite film. A representative cross-sectional SEM image (f), the best J−V data (g) and histogram of cell efficiencies among 30 cells (h) produced by mesoporous PbI_2 film.

was produced by the same thermal treatment on the PbI_2:DMF precursor film due to the easy escape of coordinative DMF (Figure S9). High-quality perovskite films were readily prepared by reacting the mesoporous PbI_2 films with MAI (Figure 4d and S9). In such a protocol, the formation of Pb_3I_8 was not detected (Figure 4e and S11). As monitored by SEM (Figure S12), there was negligible change in the films' thickness when MAI was dropped onto the mesoporous PbI_2 films to allow them to be fully converted into perovskite films. In contrast, the reaction of MAI with the PbI_2 layer made in the absence of DMSO showed a double thickness expansion due to the lattice expansion from PbI_2 to perovskite. High-performance PSCs were readily fabricated from the mesoporous PbI_2 films derived from either PbI_2:DMSO or PbI_2:2DMSO precursors. The as-fabricated solar cells all displayed a better performance (17.6 ± 1.0%) than that made by the reported two-step method (16.6 ± 1.2%) in reverse scan (Figure 4f,g, S13a and Table S2). However, it should be noted that a relatively broader distribution (16.6 ± 1.5%) in forward scan was still observed, although it is already less than that (15.5 ± 2.1%) by the reported two-step method (Figure 4h and S13b).

I-Rich Ionic Compounds. The amount of MAI drop-casted in the films is also critical to the formation of high-quality pervoskite films. In this study, perovskite films prepared by the one-step method with different PbI_2-MAI ratios were investigated. For the samples before annealing, when MAI-PbI_2 ratio was 2, the formation of pervoskite was readily observed, as evidenced by the black color of prepared films (Figure S14) and XRD patterns (Figure 5a and S15). It is

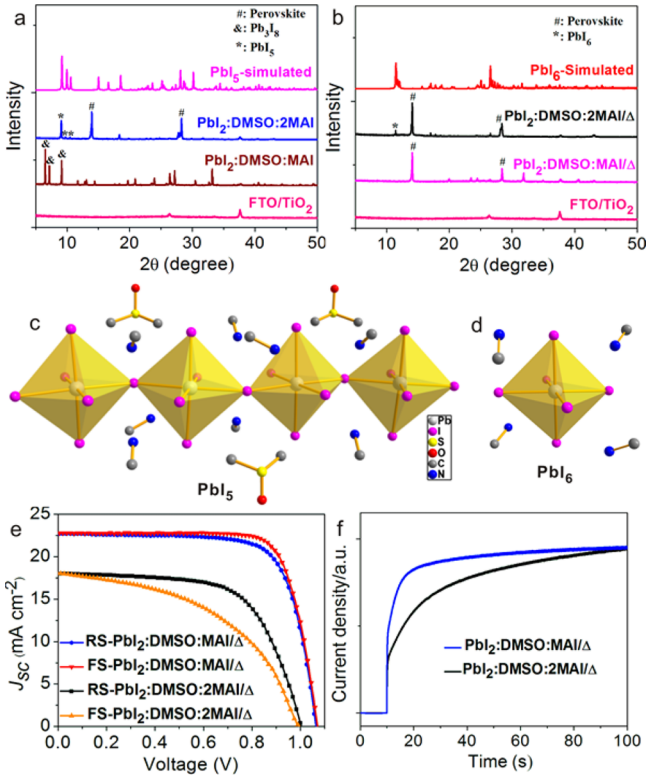

Figure 5. XRD spectra of the films with MAI-PbI_2 ratio of 1 and 2 before (a) and after (b) annealing (Δ). Crystal structures of PbI_5 (c) and PbI_6 (d). The best J−V data in forward (FS) and reverse (RS) scans (e), and the dynamic J_{sc} transient processes poled with −1 V switching bias voltage (f) for the devices.

particularly interesting that a new phase also formed different from the formation of intermediate Pb_3I_8 phase in the film prepared with MAI-PbI_2 ratio of 1. In order to identify this new phase, the single crystals suitable for X-ray diffraction were recrystallized by diffusing CH_2Cl_2 into the DMF solution of PbI_2, MAI and DMSO with the molar ratio of 1:3:1. As shown in Figure 5c, this new phase had a I-rich composition of $(MA)_3PbI_5$ (denoted as PbI_5).The structure of PbI_5 can be described as anionic single-chains of corner-sharing PbI_6 octahedra that are separated by MA cations. A good match between the experimental and simulated XRD patterns (Figure S15) was observed. When the MAI-PbI_2 ratio was further increased to 3 and 4, another I-rich phase started to form with the disappearance of perovskite phase, evidenced by the color change from black to yellow again and corresponding XRD patterns (Figure S14 and S15). The new phase can be designed as $(MA)_4PbI_6$ (denoted as PbI_6), demonstrated by the perfect

DOI: 10.1021/jacs.6b04924
J. Am. Chem. Soc. 2016, 138, 9919−9926

match of experimental XRD pattern and simulated pattern from the crystal structure of PbI_6 reported by other group (Figure S15).[35] PbI_6 contains individual PbI_6 octahedra with charges balanced by MA (Figure 5d). After thermal annealing, the PbI_6 phase was clearly observed for all films prepared with excess MAI (Figure 5b and S16). As shown in SEM images (Figure S17), no obvious crystalline domains can be visualized on the surface of these films either before or after annealing compared to the films prepared using equimolar ratio of MAI and PbI_2. The performance measurements revealed a prominent hysteresis in the representative PSC device fabricated with PbI_2:2MAI (Figure 5e and Table S3). The dynamic J_{sc} transient process analyses after electric poling were carried out on this cell to understand the above phenomena.[40] The device fabricated using the equal molar ratio of MAI and PbI_2 was also measured for comparison. As shown in Figure 5f and S18, J_{sc} values for poled devices in pseudosteady state gradually increased to the same values as that in the unpoled devices within 100 s. However, the device fabricated based on PbI_2:2MAI exhibited remarkably slow recovery speed. It is reasonable to argue that the existence of I-rich ionic compound (PbI_6) in the perovskite film prepared by the nonstoichiometry of PbI_2 and MAI could yield accumulated ions at the interface under electric poling. Consequently, the anomalous hysteresis would be induced (Figure 5e).

Removing I-Rich Impurities to Reduce Hysteresis. Considering that the presence of I-rich ionic compound PbI_6 could be one of the reasons for the hysteresis in PSCs, the removal of this compound would help to reduce the hysteresis. Then IPA was proposed to wash the synthesized PbI_6 powder sample obtained by adding CH_2Cl_2 into the DMF solution of PbI_2 and MAI with molar ratio of 1:4. The purity of powder sample was demonstrated by the perfect match between measured XRD pattern of as-prepared powder and the simulated pattern from crystal structure of PbI_6 (Figure 6b).[35] It is interesting that the conversion of PbI_6 to perovskite

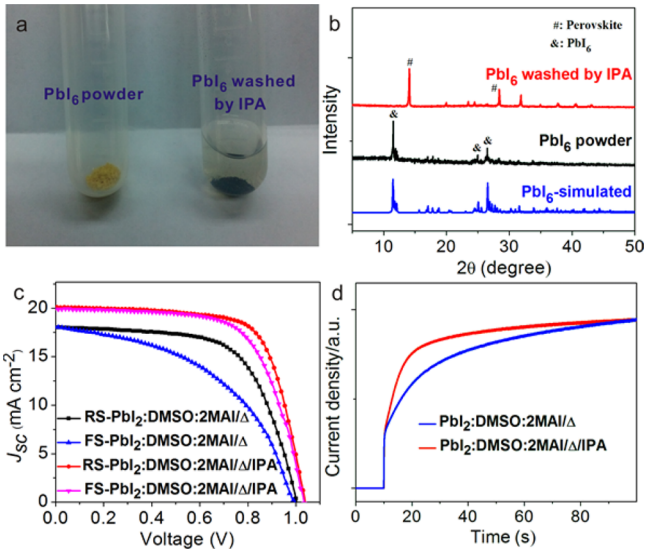

Figure 6. (a) The photograph of the PbI_6 powder before (Left) and after (Right) washing by IPA, and corresponding XRD spectra (b).The best J–V data in forward (FS) and reverse (RS) scans (c), and the dynamic J_{sc} transient processes poled with −1 V switching bias voltage for the devices with MAI-PbI_2 ratio of 2 before and after IPA washing (d).

can be well fulfilled, as evidenced by the obtained black color of the powder (Figure 6a) and XRD patterns (Figure 6b). During this process, PbI_6 ($(MA)_4PbI_6$) was decomposed to perovskite and MAI with the help of IPA. MAI was dissolved into IPA solution and removed, thus yielding the pure perovskite. Also, the surface morphology of the IPA-treated perovskite films became much distinct with highly crystalline domains as displayed in the representative film obtained by PbI_2:2MAI (Figure S19). As expected, the decreased hysteresis was observed (Figure 6c and Table S3) in the corresponding fabricated PSCs. The largely reduced hysteresis was also demonstrated by the obviously improved recovery speed of J_{sc} value in the J-V curve for poled sample in pseudosteady state (Figure 6d and Figure S20). In fact, when the MAI-PbI_2 ratio was above 1.2, I-rich ionic compounds were already detectable (Figure S21, 22). When the IPA treatment was employed to the as-obtained perovskite films by the nonstoichiometry reaction of mesoporous PbI_2 scaffold with MAI in our two-step method (Figure 4), a further decreased hysteresis (17.0 ± 1.1%, compared to 16.6 ± 1.5% before IPA washing) in the forward scan were also accomplished (Figure S23).

Optimizing Domain Size by Reaction Dynamics. To achieve sufficient conversion of mesoporous PbI_2 into perovskite, a high concentration of MAI with 50 mg/mL was used (Figure S24). However, such a high concentration MAI led to a relatively rough perovskite morphology with small grain size (~700 nm, Figure 4d) due to the formation of abundant nuclei.[21] To construct large-scale perovskite films, the manipulation of reaction dynamics between reactant molecules (PbI_2 and MAI) is important. As shown in Figure 7a–c, immersing the as-prepared mesoporous PbI_2 film into a hot MAI solution with a lower concentration (10 mg/mL) helped to create a MAI-rich reaction environment to achieve the complete conversion of PbI_2 to perovskite. After the conversion, the film was immersed into IPA solution about 30 s to remove the excess I-rich ionic compound PbI_6 (Figure S25), generating a pure and smooth perovskite film with ~1–2 μm large-scale grains (Figure 7d,e). The reaction of high concentration of MAI (50 mg/mL) with mesoporous PbI_2 film gave an easy formation of PbI_6 intermediate (Figure S26), and generated a relatively rough perovskite morphology with small grain sizes (Figure S27). The performance measurement revealed the best efficiency up to 19.0% on the devices fabricated from the above obtained high-quality perovskite films (Figure 7f,g, S28 and Table S4). To verify the performance of the PSC, the stabilized efficiency output of 18.5% (Figure S29) was monitored over 200 s near the maximum power point. A narrow distribution and negligible hysteresis (18.0 ± 1.0% for reverse scan and 17.4 ± 1.0% for forward scan) were also achieved (Figure 7h).

■ CONCLUSION

The molecular reaction between PbI_2 and MAI with the introduction of DMSO was investigated in details. Five different possible intermediates were captured and structurally analyzed by X-ray single-crystals analyses. The following several findings of this study help to develop high-quality perovskite films for reproducible PSCs: (1) The formation of the Pb_3I_8 intermediate was NOT the key factor for the fabrication of high-quality pervoskite films. (2) The different PbI_2:DMSO ratio led to the formation of two PbI_2-DMSO precursors of different structures. (3) The incorporation of DMSO into the PbI_2 precursors facilitated the fabrication of high-quality PbI_2

DOI: 10.1021/jacs.6b04924
J. Am. Chem. Soc. 2016, 138, 9919–9926

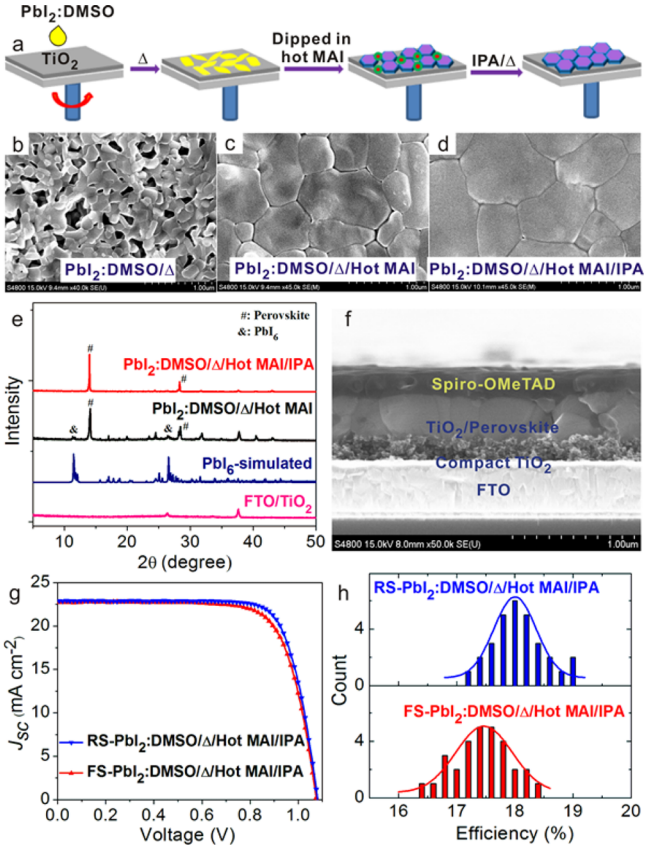

Figure 7. (a) Schematic illustration of cell fabrication process. SEM images (b–d) and XRD patterns (e) of the reaction process for mesoporous PbI_2 with hot MAI solution. Cross-sectional SEM image (f) and the best J–V data (g) of an optimized PSC, and the histogram of efficiencies for 30 cells in forward (FS) and reverse (RS) scans (h).

precursor films. (4) The use of excess amount of MAI easily led to the formation of I-rich phases, such as PbI_5 and PbI_6, while these compounds were transferred to PbI_6 after annealing. The presence of PbI_6 in the perovskite films aggravated the hysteresis issue in PSCs. (5) Once treated with isopropanol, PbI_6 was readily converted into perovskite. On the basis of these findings, a new highly reproducible protocol to fabricate high-performance PSCs has been developed. In the new protocol, high-quality perovskite films were prepared by simply treating the mesoporous PbI_2 films (made from PbI_2-DMSO precursors) with an isopropanol solution of MAI, followed by isopropanol washing. The best efficiency of fabricated $MAPbI_3$ PSCs was up to 19.0%. As compared to the previously reported DMSO method, PSCs fabricated by the method developed in this work display narrow efficiency distributions. And the efficiency difference between forward and reverse scans is much smaller.

EXPERIMENTAL SECTION

Materials. All chemicals and reagents were used as received from chemical companies without any further purification. The MAI was synthesized and purified according to the literature method.[2] To a stirred solution of methylamine in methanol (40 wt %, 24 mL) aqueous hydroiodic acid (57 wt %, 25 mL) was slowly added at 0 °C. After 2 h, the precipitate was collected by evaporation at 50 °C for 1 h. The as-obtained product was washed with diethyl ether three times and then finally dried at 60 °C in a vacuum oven for 24 h to afford the desired pure MAI as white crystals.

Solar Cell Fabrications. Fluorine-doped Tin Oxide (FTO) glass substrates in the dimension of 2.0 cm × 2.0 cm were patterned by etching with zinc powder and 2 M hydrochloric acid. The substrates were then sequentially washed in ultrasonic baths of acetone, distilled water and ethanol. A compact TiO_2 blocking layer was spin-coated onto the cleaned FTO glass using 0.15 M titanium tetraisopropanolate in ethanol solution at 2000 rpm for 30 s. The substrate was then annealed at 550 °C for 30 min. After cooling to room temperature, the film was immersed into the 20 mM $TiCl_4$ solution at 70 °C for 30 min. After dried, a ∼150 nm thick mesoporous TiO_2 film was deposited on the pretreated FTO substrate by spin-coating of the TiO_2 paste (Dyesol DSL 18NR-T) with ethanol (1:5, mass ratio), which was followed by the heating at 550 °C for 30 min.

The perovskite layers were first fabricated on TiO_2 by reported one- and two-step methods. In a typical one-step protocol, a mixture of 461 mg of PbI_2, 159 mg of MAI, 78 mg of DMSO (molar ratio 1:1:1) and 600 mg of DMF was prepared at room temperature and stirred for 1 h. The completely dissolved precursor solution was spin-coated on the prepared FTO substrate at 4000 rpm for 25 s, when 0.5 mL of diethyl ether was slowly dripped on the rotating substrate in 8 s. The obtained transparent film was then heated at 70 °C for 1 min and 100 °C for 2 min to form a dense $MAPbI_3$ film. In the two-step method, a mixture of 461 mg of PbI_2 and 78 mg of DMSO (molar ratio 1:1) dissolved in 600 mg of DMF was spin-coated on the prepared FTO substrate at 3000 rpm for 25 s. Subsequently, the solution of MAI in isopropanol (50 mg/mL) was directly dropped on the substrate for 15 s loading time to achieve the complete conversation of PbI_2, which was spun at 3000 rpm for 10 s and then heated at 120 °C for 20 min.

In this study, two different methods based on mesoporous PbI_2 were also developed for the fabrication of perovskite layers. Perovskite was formed by reacting mesoporous PbI_2 with MAI in the solid form or solution. In the method based on solid–solid reaction, a mixture of 461 mg of PbI_2 and 78 mg of DMSO (molar ratio 1:1) dissolved in 600 mg of DMF was spin-coated on the prepared FTO substrate at 3000 rpm for 25 s. The films were annealed at 80 °C for 5 min to prepare the mesoporous PbI_2 film. After cooling to room temperature, the solution of MAI in isopropanol (50 mg/mL) was directly dropped on the substrate for 7 s loading time, and then spun at 3000 rpm for 10 s. Finally, the substrate was heated at 120 °C for 5 min. In the method based on solid-solution reaction, the prepared mesoporous PbI_2 film was dipped into the hot solution (70 °C) of MAI in isopropanol (10 mg/mL) for 2 min. After that, the film was immersed into IPA solution about 30 s to remove the I-rich ionic compounds and then heated at 100 °C for 5 min.

After the preparation of perovskite layer, the hole transport layer solution was coated by solution process at 4000 rpm for 30 s, where Spiro-OMeTAD/chlorobenzene (72 mg/1 mL) solution was employed with the additives containing 17.5 μL Li-TFSI/acetonitrile (520 mg/1 mL) and 28.8 μL TBP. Finally, a 80 nm thick Au counter electrode was deposited by thermal evaporation under reduced pressure of 2×10^{-7} Torr. The active area was 0.11 cm^2.

Preparation of Intermediate Samples. Preparation of PbI_2·2DMSO crystals: PbI_2 was dissolved in DMSO and then toluene was slowly diffused into above solution to generate colorless crystals.

Preparation of PbI_2·DMSO crystals: PbI_2 was dissolved in DMSO and then toluene was slowly added. The obtained white precipitation was filtered and annealed in vacuum oven at 60 °C for 24 h. The obtained powder was redissolved into DMF and then ethanol was slowly diffused into above solution to get colorless crystals.

Preparation of PbI_2·DMF crystals: PbI_2 was dissolved in DMF and then acetone was slowly diffused into above solution to generate colorless crystals.

Preparation of Pb_3I_8 crystals: PbI_2 and MAI with molar ratio of 1:1 were dissolved in DMSO and then diethyl ether was slowly diffused into above solution to obtain yellow crystals.

Preparation of PbI_5 crystals: PbI_2, MAI and DMSO with the molar ratio of 1:3:1 were dissolved in DMF and then CH_2Cl_2 was slowly diffused into above solution to yield yellow crystals.

DOI: 10.1021/jacs.6b04924
J. Am. Chem. Soc. 2016, 138, 9919–9926

Preparation of PbI_6 powder: PbI_2 and MAI with molar ratio of 1:4 were dissolved in DMF and then CH_2Cl_2 was slowly added into above solution to give yellow powder samples.

Device Characterizations. The current−voltage characteristics were recorded from a solar simulator equipped with a Keithley 2400 source meter and 300 W collimated xenon lamp (Newport) calibrated with the light intensity to 100 $mW{\cdot}cm^{-2}$ at AM 1.5 G solar light condition by the certified silicon solar cell. Incident photon-to-electron conversion efficiency (IPCE) was measured on a computer-controlled IPCE system (Newport) containing a xenon lamp, a monochromator and a Keithley multimeter. The system was calibrated with the certified silicon solar cell and the IPCE data were collected at DC mode. XRD patterns were analyzed by an X-ray diffractometer (Rigaku, RINT-2500) with a Cu Ka radiation source. The surface morphology of were recorded via a SEM-4800 field-emission scanning electron microscope (SEM).

Single-Crystal Analysis. The photos of the obtained crystals were shown in Figure S30. The diffraction data of all crystals was collected on an Agilent Technologies SuperNova system using Mo Kα radiation (λ = 0.71073 Å) for $PbI_2{\cdot}2DMSO$, $PbI_2{\cdot}DMSO$, $PbI_2{\cdot}DMF$ and Pb_3I_8, and Cu Kα radiation (λ = 1.5418 Å) for PbI_5 microfocus X-ray sources at 100 K. The data was processed using CrysAlis.[41] The structure was solved and refined using Full-matrix least-squares based on F^2 with program *SHELXS-97* and *SHELXL-97* within *Olex2*.[42,43] The detailed crystallographic data and structure refinements were given in Table S5.

■ ASSOCIATED CONTENT

Supporting Information

The Supporting Information is available free of charge on the ACS Publications website at DOI: 10.1021/jacs.6b04924.

Details of the XRD, SEM images and photovoltaic performances of the devices (PDF)
Crystallographic data for $PbI_2{\cdot}2DMSO$ (CIF)
Crystallographic data for $PbI_2{\cdot}DMSO$ (CIF)
Crystallographic data for $PbI_2{\cdot}DMF$ (CIF)
Crystallographic data for Pb_3I_8 (CIF)
Crystallographic data for PbI_5 (CIF)

■ AUTHOR INFORMATION

Corresponding Authors

*lijing@xmu.edu.cn
*nfzheng@xmu.edu.cn

Author Contributions

§J. Cao and X.-J. Jing contributed equally to this work.

Notes

The authors declare no competing financial interest.

■ ACKNOWLEDGMENTS

We thank the NSFC of China (21420102001, 21131005, 21390390, 21333008, 21401156) for financial support.

■ REFERENCES

(1) Kojima, A.; Teshima, K.; Shirai, Y.; Miyasaka, T. *J. Am. Chem. Soc.* **2009**, *131*, 6050.
(2) Im, J. H.; Lee, C. R.; Lee, J. W.; Park, S. W.; Park, N. G. *Nanoscale* **2011**, *3*, 4088.
(3) Kim, H. S.; Lee, C. R.; Im, J. H.; Lee, K. B.; Moehl, T.; Marchioro, A.; Moon, S. J.; Humphry-Baker, R.; Yum, J. H.; Moser, J. E.; Gratzel, M.; Park, N. G. *Sci. Rep.* **2012**, *2*, 1.
(4) Lee, M. M.; Teuscher, J.; Miyasaka, T.; Murakami, T. N.; Snaith, H. J. *Science* **2012**, *338*, 643.
(5) Liu, M.; Johnston, M. B.; Snaith, H. J. *Nature* **2013**, *501*, 395.
(6) Mei, A.; Li, X.; Liu, L.; Ku, Z.; Liu, T.; Rong, Y.; Xu, M.; Hu, M.; Chen, J.; Yang, Y.; Grätzel, M.; Han, H. *Science* **2014**, *345*, 295.
(7) Zhou, H.; Chen, Q.; Li, G.; Luo, S.; Song, T. B.; Duan, H. S.; Hong, Z.; You, J.; Liu, Y.; Yang, Y. *Science* **2014**, *345*, 542.
(8) Jeon, N. J.; Noh, J. H.; Yang, W. S.; Kim, Y. C.; Ryu, S.; Seo, J.; Seok, S. I. *Nature* **2015**, *517*, 476.
(9) Nie, W.; Tsai, H.; Asadpour, R.; Blancon, J.-C.; Neukirch, A. J.; Gupta, G.; Crochet, J. J.; Chhowalla, M.; Tretiak, S.; Alam, M. A.; Wang, H.-L.; Mohite, A. D. *Science* **2015**, *347*, 522.
(10) Yang, W. S.; Noh, J. H.; Jeon, N. J.; Kim, Y. C.; Ryu, S.; Seo, J.; Seok, S. I. *Science* **2015**, *348*, 1234.
(11) Abate, A.; Saliba, M.; Hollman, D. J.; Stranks, S. D.; Wojciechowski, K.; Avolio, R.; Grancini, G.; Petrozza, A.; Snaith, H. J. *Nano Lett.* **2014**, *14*, 3247.
(12) Zhu, Z.; Ma, J.; Wang, Z.; Mu, C.; Fan, Z.; Du, L.; Bai, Y.; Fan, L.; Yan, H.; Phillips, D. L.; Yang, S. *J. Am. Chem. Soc.* **2014**, *136*, 3760.
(13) Cao, J.; Liu, Y. M.; Jing, X. J.; Yin, J.; Li, J.; Xu, B.; Tan, Y. Z.; Zheng, N. F. *J. Am. Chem. Soc.* **2015**, *137*, 10914.
(14) Cao, J.; Yin, J.; Yuan, S. F.; Zhao, Y.; Li, J.; Zheng, N. F. *Nanoscale* **2015**, *7*, 9443.
(15) Liu, L. F.; Mei, A. Y.; Liu, T. F.; Jiang, P.; Sheng, Y. S.; Zhang, L. J.; Han, H. W. *J. Am. Chem. Soc.* **2015**, *137*, 1790.
(16) Zuo, L.; Gu, Z.; Ye, T.; Fu, W.; Wu, G.; Li, H.; Chen, H. *J. Am. Chem. Soc.* **2015**, *137*, 2674.
(17) Eperon, G. E.; Stranks, S. D.; Menelaou, C.; Johnston, M. B.; Herz, L. M.; Snaith, H. J. *Energy Environ. Sci.* **2014**, *7*, 982.
(18) Arora, N.; Dar, M. I.; Hezam, M.; Tress, W.; Jacopin, G.; Moehl, T.; Gao, P.; Aldwayyan, A. S.; Deveaud, B.; Grätzel, M.; Nazeeruddin, M. K. *Adv. Funct. Mater.* **2016**, *26*, 2846.
(19) Yang, S.; Wang, Y.; Liu, P.; Cheng, Y.-B.; Zhao, H. J.; Yang, H. G. *Nature Energy* **2016**, *1*, 15016.
(20) Chen, Q.; Zhou, H.; Hong, Z.; Luo, S.; Duan, H.-S.; Wang, H.-H.; Liu, Y.; Li, G.; Yang, Y. *J. Am. Chem. Soc.* **2014**, *136*, 622.
(21) Im, J.-H.; Jang, I.-H.; Pellet, N.; Grätzel, M.; Park, N.-G. *Nat. Nanotechnol.* **2014**, *9*, 927.
(22) Xiao, Z.; Dong, Q.; Bi, C.; Shao, Y.; Yuan, Y.; Huang, J. *Adv. Mater.* **2014**, *26*, 6503.
(23) Liu, Y.; Hong, Z.; Chen, Q.; Chang, W.; Zhou, H.; Song, T. B.; Young, E.; Yang, Y. M.; You, J.; Li, G.; Yang, Y. *Nano Lett.* **2015**, *15*, 662.
(24) Song, T.-B.; Chen, Q.; Zhou, H.; Jiang, C.; Wang, H.-H.; Yang, Y.; Liu, Y.; You, J.; Yang, Y. *J. Mater. Chem. A* **2015**, *3*, 9032.
(25) Yan, K.; Long, M.; Zhang, T.; Wei, Z.; Chen, H.; Yang, S.; Xu, J. *J. Am. Chem. Soc.* **2015**, *137*, 4460.
(26) Zhang, T.; Yang, M.; Zhao, Y.; Zhu, K. *Nano Lett.* **2015**, *15*, 3959.
(27) Sharenko, A.; Toney, M. F. *J. Am. Chem. Soc.* **2016**, *138*, 463.
(28) Jeon, N. J.; Noh, J. H.; Kim, Y. C.; Yang, W. S.; Ryu, S.; Seok, S. I. *Nat. Mater.* **2014**, *13*, 897.
(29) Wu, Y.; Islam, A.; Yang, X.; Qin, C.; Liu, J.; Zhang, K.; Peng, W.; Han, L. *Energy Environ. Sci.* **2014**, *7*, 2934.
(30) Ahn, N.; Son, D.-Y.; Jang, I.-H.; Kang, S. M.; Choi, M.; Park, N.-G. *J. Am. Chem. Soc.* **2015**, *137*, 8696.
(31) Li, W.; Fan, J.; Li, J.; Mai, Y.; Wang, L. *J. Am. Chem. Soc.* **2015**, *137*, 10399.
(32) Guo, Y.; Shoyama, K.; Sato, W.; Matsuo, Y.; Inoue, K.; Harano, K.; Liu, C.; Tanaka, H.; Nakamura, E. *J. Am. Chem. Soc.* **2015**, *137*, 15907.
(33) Rong, Y.; Tang, Z.; Zhao, Y.; Zhong, X.; Venkatesan, S.; Graham, H.; Patton, M.; Jing, Y.; Guloy, A. M.; Yao, Y. *Nanoscale* **2015**, *7*, 10595.
(34) Rong, Y.; Venkatesan, S.; Guo, R.; Wang, Y.; Bao, J.; Li, W.; Fan, Z.; Yao, Y. *Nanoscale* **2016**, *8*, 12892.
(35) Wakamiya, A.; Endo, M.; Sasamori, T.; Tokitoh, N.; Ogomi, Y.; Hayase, S.; Murata, Y. *Chem. Lett.* **2014**, *43*, 711.
(36) Miyamae, H.; Numahata, Y.; Nagata, M. *Chem. Lett.* **1980**, *9*, 663.
(37) Zhang, H.; Mao, J.; He, H.; Zhang, D.; Zhu, H. L.; Xie, F.; Wong, K. S.; Grätzel, M.; Choy, W. C. H. *Adv. Energy Mater.* **2015**, *5*, 1501354.

DOI: 10.1021/jacs.6b04924
J. Am. Chem. Soc. 2016, 138, 9919−9926

(38) Liu, T.; Hu, Q.; Wu, J.; Chen, K.; Zhao, L.; Liu, F.; Wang, C.; Lu, H.; Jia, S.; Russell, T.; Zhu, R.; Gong, Q. *Adv. Energy Mater.* **2016**, *6*, 1501890.
(39) Yi, C.; Li, X.; Luo, J.; Zakeeruddin, S. M.; Gratzel, M. *Adv. Mater.* **2016**, *28*, 2964.
(40) Chen, B.; Yang, M.; Zheng, X.; Wu, C.; Li, W.; Yan, Y.; Bisquert, J.; Garcia-Belmonte, G.; Zhu, K.; Priya, S. *J. Phys. Chem. Lett.* **2015**, *6*, 4693.
(41) *CrysAlisPro*, Version 1.171.35.19; Agilent Technologies Inc.: Santa Clara, CA, 2011.
(42) Sheldrick, G. M. *Acta Crystallogr., Sect. A: Found. Crystallogr.* **2008**, *64*, 112.
(43) Dolomanov, O. V.; Bourhis, L. J.; Gildea, R. J.; Howard, J. A.; Puschmann, H. *J. Appl. Crystallogr.* **2009**, *42*, 339.

DOI: 10.1021/jacs.6b04924
J. Am. Chem. Soc. 2016, 138, 9919−9926